ADVANCED FUNCTIONAL MATERIALS
www.afm-journal.de

N-Dihydrogalactochitosan Drives Conventional and Alternative Activations of STING to Synergize Type I IFN and IL-1β Productions for Antitumor Immunity.

Ashley R. Hoover, Kaili Liu, Coline Furrer, Samuel Siu Kit Lam, David W. Anderson, Zhijun Zhou, Jingxuan Yang, Chun Fung Wong, Alexandra D. Medcalf, Xiao-Hong Sun, Tomas Hode, Lu Alleruzzo, Abby Delawder, Joseph Raker, Ghainaa Abousleiman, Trisha I. Valerio, Yuanhong Sun, James F. Papin, Min Li, and Wei R. Chen**

_N_-dihydrogalactochitosan (GC) is an immune stimulant/adjuvant. Synthesized from chitosan and galactose, GC is a new chemical entity that significantly enhances the immune-stimulating properties of its parental material, chitosan, making it a promising therapeutic agent. When used in combination with antigenic material, GC stimulates innate and adaptive antitumor and antiviral immunities. However, its mechanism has not been fully investigated. Herein it is demonstrated that GC drives type I IFN activation in antigen-presenting cells (APCs). More importantly, GC drives alternative STING pathways, leading to inflammatory cell death that enhances dendritic cell (DC) activation. GC-activated DCs trigger a variety of nucleic acid sensing pattern recognition receptors (PRRs) pathways and IL-1β production via the activation of the inflammasome. In vivo, GC induces a potent response of type I IFNs and upregulates genes associated with STING signaling within the tumor microenvironment (TME). Moreover, intratumoral delivery of GC reduces the numbers of M2-like macrophages and increases M1-like macrophages residing within the TME, while subsequently increasing the number of activated DCs. This findings demonstrate that GC acts as a multimodal immune stimulant via STING to generate a broad type I IFN response. This uniquely broad response holds therapeutic promise in generating enhanced antitumor and antiviral immunities.

1. Introduction

N-dihydrogalactochitosan (GC) is a novel immunostimulant/adjuvant synthesized using galactose and partially acetylated glucosamine polymer chitosan (Immunophotonics-001; IP-001). Chitosan, in turn, is derived from chitin, which is largely extracted from the shells of crustaceans, and is a polymer that consists of *N*-acetylglucosamine.[1] Chitosan is a nontoxic, biodegradable, biocompatible, natural polysaccharide, currently used in a variety of chemical, biotechnological, pharmacological, and medicinal technologies.[2] Carroll et al, revealed that using chitosan as a vaccine adjuvant enhanced cellular- and humoral-mediated immunity and drove a type I interferon (IFN) response through stimulator of interferon genes (STING) signaling.[3] STING agonists, such as cyclic dinucleotides, lead to enhanced humoral and cellular immunity capable of preventing and eliminating

A. R. Hoover, K. Liu, C. Furrer, G. Abousleiman, T. I. Valerio, Y. Sun, W. R. Chen
Stephenson School of Biomedical Engineering
University of Oklahoma
Norman, OK 73019, USA
E-mail: Wei-R-Chen@ou.edu

A. R. Hoover, A. D. Medcalf, X.-H. Sun
Arthritis and Clinical Immunology Research Program
Oklahoma Medical Research Foundation
Oklahoma City, OK 73104, USA

The ORCID identification number(s) for the author(s) of this article can be found under https://doi.org/10.1002/adfm.202410079

DOI: 10.1002/adfm.202410079

S. S. K. Lam, D. W. Anderson, C. F. Wong, T. Hode, L. Alleruzzo, A. Delawder, J. Raker
Immunophotonics
Inc.
St. Louis, MO 63110, USA

Z. Zhou, J. Yang, M. Li
Department of Medicine
Department of Surgery
University of Oklahoma Health Sciences Center
Oklahoma City, OK 73104, USA
E-mail: Min-Li@ouhsc.edu

J. F. Papin
Department Pathology and Division of Comparative Medicine
University of Oklahoma Health Sciences Center
Oklahoma City, OK 73104, USA

M. Li, W. R. Chen
Stephenson Cancer Center
University of Oklahoma Health Sciences Center
Oklahoma City, OK 73104, USA

intracellular pathogen infections following vaccination and generating protective cellular immunity against tumors, making them highly desirable for stimulating sustained and protective immune responses.[4] However, the cyclic dinucleotides must be administered repeatedly, in high quantities, and/or modified to prevent host cell inactivation, especially when delivered systemically.[4a,b,5] The fact that chitosan stimulates STING signaling and other immune pathways makes it a potential immune stimulant for cancer immunotherapy. However, due to its poor solubility at a neutral pH, its poorly understood structure-activity relationship, the potential contributions of endotoxins to its observed activity, and the difficulty in appropriately characterizing the polymeric mixture,[6] the potential of chitosan as a clinically relevant immune stimulant is limited.

To address these issues and to significantly increase the type I IFN immune responses and other immunological pathways, we developed a new chemical entity, *N*-dihydrogalactochitosan (GC), by attaching galactose to chitosan.[7] The first clinical GC drug candidate, IP-001,[8] is synthesized and purified under GMP conditions, which included comprehensive structural characterization and extensive tests for metals, endotoxins, and other impurities, further addressing the major challenges in the applications of chitosan.[6] GC/IP-001 has been safely used in early clinical trials for the treatment of solid tumors in combination with local tumor ablation.[9] Our previous studies have demonstrated that GC itself is non-toxic.[9,10] It has been utilized in combination with laser irradiation for the treatment of metastatic cancers in patients. In these clinical cases, the side effects experienced by patients are primarily attributable to thermal damage resulting from non-invasive laser irradiation. However thermal damage is recoverable. Additionally, patients exhibit signs of inflammation and flu-like symptoms following treatment. These responses are anticipated and desired, as they indicate the specific and efficient activation of anti-tumor immune activation pathways necessary for controlling tumor growth and metastasis.

We have previously demonstrated the immune-stimulating potential of GC in the context of local ablation-based immunotherapy for metastatic cancers, particularly by combining photothermal therapy (PTT) ablation and intratumoral delivery of GC.[9,11] PTT disrupts tumor homeostasis, induces tumor cell necrosis, and releases tumor-specific antigens (TSAs), while GC overcomes the largely anti-inflammatory tumor microenvironment (TME) and enhances the immune response to the released TSAs and release of molecular danger signals including tumor-derived RNA, DNA, high mobility group box-1(HMGB1,), heat shock protein (HSP,) and calreticulin (CRT).[12] Using RNA sequencing analyses, we examined the immune cells within the TME following the intratumoral application of GC and found that GC drove a strong type I interferon (IFN) response in both innate and adaptive tumor-infiltrating leukocytes (TILs). The major immune stimulation in ablation + GC treatment was potentiated by GC.[13] However, only the combination of ablation and GC was able to achieve sustained tumor regression in both treated tumors and untreated distant metastases as well as prolonged survival.[9,11]

In addition to the observed antitumor immune responses, our studies on the transcriptomic profiles of immune cells treated with GC revealed a significant upregulation of genes involved in antigen processing and presentation, type I IFN responses, and antiviral responses.[13] These results indicate that GC is a potent immunostimulant and can be used as a potential anticancer or antiviral therapeutic and/or a vaccine adjuvant. The promising immunological effect of GC and its potential for future clinical applications warrant an investigation to gain a deeper understanding of its mechanism in triggering immune system activation.

Understanding the mechanism of action of an immunostimulant or adjuvant for immunotherapy is crucial for several reasons. First, knowing how an immunostimulant or adjuvant works allows for the optimization of its use for maximum therapeutic benefit. This includes determining the best dosages, schedules, and combinations with other treatments. Additionally, understanding the mechanisms of GC aids in the identification of biomarkers, pathways, and cellular targets involved that can be used to monitor the effectiveness of therapy or predict responses. This is particularly important in immunotherapy, where responses can vary widely among patients. Different patients may respond differently to immunostimulants or adjuvants due to genetic, environmental, or disease-specific factors. Understanding the regulatory mechanisms allows for the development of personalized treatment plans tailored to individual patient profiles. Furthermore, understanding these mechanisms helps in designing combination strategies that can synergistically enhance efficacy and reduce the likelihood of resistance. Lastly, a clear understanding of GC's mechanisms can facilitate the clinical development and approval process of the drug. Therefore, understanding the mechanisms of GC-induced immune responses is foundational to advancing the field of immunotherapy, leading to better therapeutic outcomes and the development of more sophisticated and effective treatments.

In the current work, we show that GC is significantly more potent than its corresponding chitosan starting material in inducing IFNβ and the type I IFN response cytokine CXCL10 in the human monocytic cell line, THP-1. To further examine the mechanism in which GC induces type I IFN responses, we focused on the activation of dendritic cells (DCs) using murine bone marrow-derived DCs (BMDCs). In DCs, GC stimulated the production of type I IFN and IL-1β, both being dependent on STING signaling. Interestingly, we discovered STING-initiated lysosomal cell death in response to GC, leading to the activation of NLRP3 inflammasome pathway via caspase-1, and the cleavage of IL-1β and gasdermin D. RNA sequencing analysis revealed that STING played a key role in directing GC-mediated DC activation, producing cytokines, and in stimulating a variety of nucleic acid sensing pattern recognition receptors (PRRs). Furthermore, we found that GC was likely a STING stimulant because it was unable to compromise lysosomal integrity or initiate mitochondrial stress in the absence of STING.[3,14] The function of GC in initiating such a broad range of nucleic acid sensing PRRs via inflammatory cell death induction is unique and clinically significant, as most immune stimulants/adjuvants lack this combinatorial capability. Our findings demonstrate that GC can function as an effective stimulant for immunotherapy against metastatic cancers and as a potent adjuvant for vaccines against tumor antigens and intracellular pathogens.

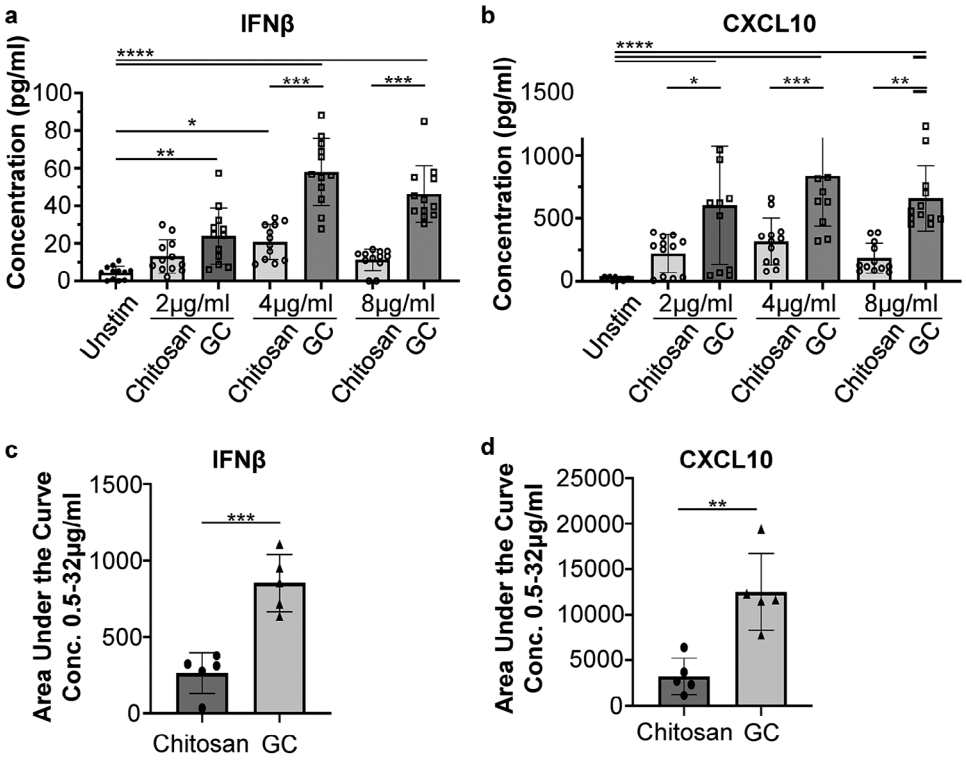

Figure 1. GC induces a stronger type I IFN response in THP-1 cells compared to chitosan. THP-1 cells were stimulated with Chitosan and GC of different concentrations for 48 h prior to analysis. A,b) Production of IFNβ and CXCL10 in the supernatant after stimulation with Chitosan and GC (2, 4, and 8 μg ml^{-1}). C,d) Total production of IFNβ and CXCL10 in the cell supernatant after stimulation using the area under the curve (AUC) for the entire range of concentrations (0.5–32 μg ml^{-1}). Data are presented as mean +/- s.e.m. n = 2 or more independent experiments. Statistical analysis was performed using one-way analysis of variance (one-way-ANOVA). *$p < 0.05$, **$p < 0.005$, ***$p < 0.0005$, ****$p < 0.00005$.

2. Results

2.1. GC Enhances the Activation of THP-1 Cells over Chitosan

To compare the similarities and potency of GC with its corresponding starting material chitosan, we stimulated human THP-1 cells,[15] which resemble monocytes and macrophages in morphology and differentiation properties, with chitosan and GC of varying concentrations for 48 h (**Figure 1**; Figure S1, Supporting Information). Following the stimulation, we found that GC induced greater amounts of IFNβ production from THP-1 cells compared to chitosan across a range of concentrations (Figure 1a and c; Figure S1a,b, Supporting Information). Complementary to type I IFN, CXCL10 production was also significantly higher in the GC-stimulated THP-1 cells across a range of concentrations (Figure 1b and d; Figure S1c,d, Supporting Information). This suggests that the addition of galactose to chitosan enhances chitosan's ability to induce type I IFN production and interferon-stimulated genes (ISG). To confirm this finding and to capture the total potency of GC, we graphed the area under the curve (AUC) for the entire range of concentrations (0.5–32 μg ml^{-1}) for both IFNβ and CXCL10 in the GC- and chitosan-stimulated THP-1 cells (Figure 1c and d). AUC analysis of both IFNβ and CXCL10 revealed that GC was significantly more potent than chitosan in stimulating type I IFN and IFN responses in THP-1 cells across a broad range of concentrations (Figure 1c and d).

2.2. GC Directly Activates Unpolarized Bone Marrow-Derived Dendritic Cells (BMDCs) to Produce type I IFNs and IL-1β

Since type I IFN-driven immune responses are critical for antitumor immune immunity[16] and for the elimination of viral infections,[17] and also since our in vitro experiments have ruled out APC-independent, non-specific T cell activation by GC alone,[18] we investigated whether GC directly activates DCs to produce type I IFN similarly to the THP-1 cells. GC of varying concentrations was used to stimulate naive bone marrow-derived dendritic cells (BMDCs) to determine the optimal GC concentration (**Figure 2a**). At the concentration of 4 μg ml^{-1}, the mean fluorescent intensities (MFI) of cell surface molecules CD86, CD40, and MHC-II were increased significantly (Figure 2b), signaling maturation and activation of the DCs. The production level of IFNβ induced by GC at 4 μg ml^{-1} was comparable to that of a known STING agonist, 2′3-cGAMP at 200 ng ml^{-1} (Figure 2c). In addition, GC induced the production of the proinflammatory cytokine IL-1β (Figure 2d), which correlates with the upregulation of CD86, CD40, and MHC-II (Figure 1b). A lower dose of GC (0.8 μg ml^{-1}) was also able to stimulate the production of IFNβ, but not IL-1β and DC maturation (CD86, CD40, and MHC-II), as shown in Figure 2a–d. Interestingly, the initiation of BMDC cell death correlated with the production of IL-1β, but not IFNβ, suggesting that the production of the two critical cytokines may be independent of each other and dependent on GC dose (Figure 2c–e).

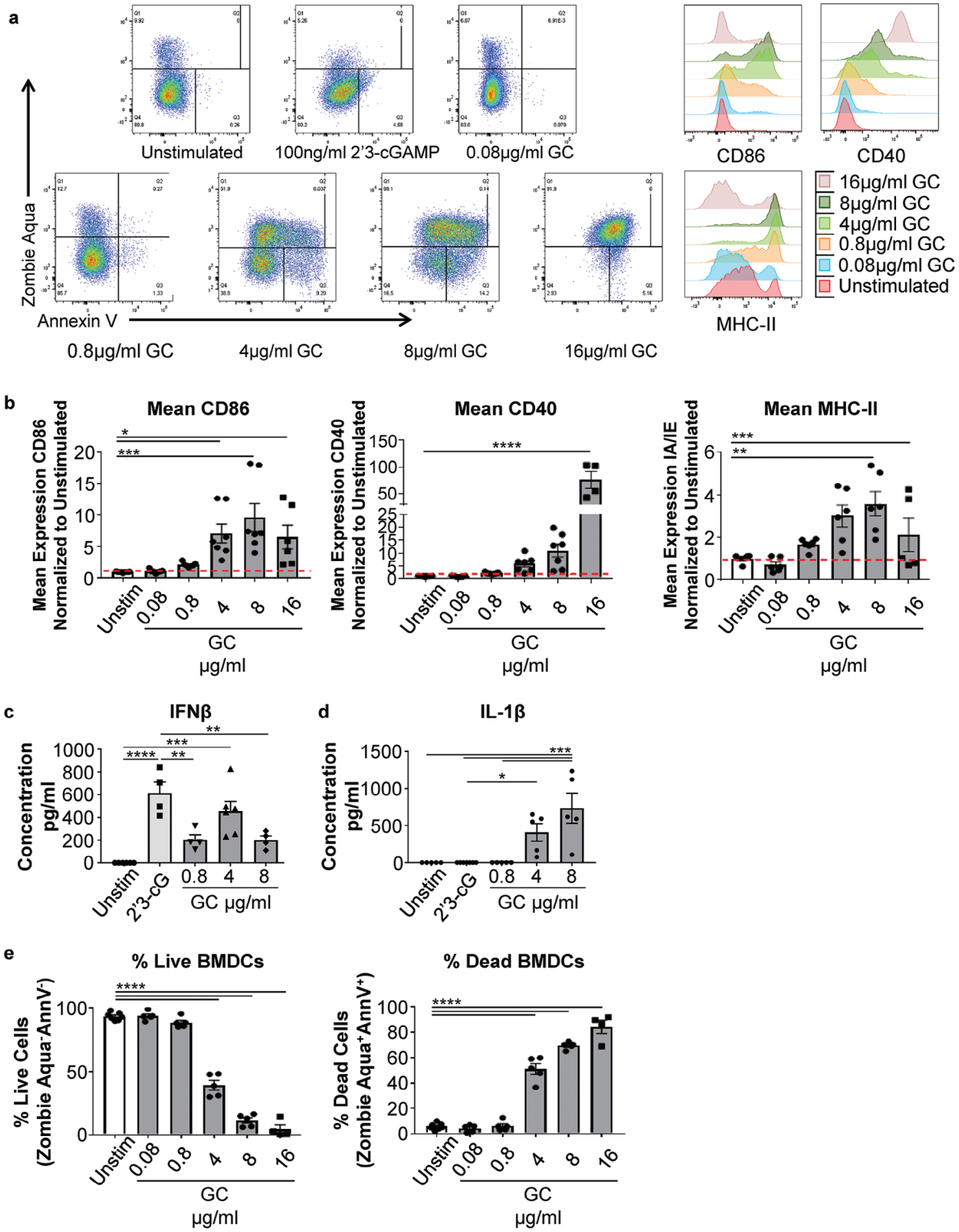

Figure 2. GC directly activates naïve mouse BMDCs and drives the production of Type I IFN and IL-1β. a) Mean expressions of CD86, CD40, and MHC-II of live BMDCs after stimulation by GC of various concentrations for 24 h. Events were pregated on leukocytes/singlets/CD11b$^+$CD11c$^+$ cells. b) Mean expressions of CD86, CD40, and MHC-II, normalized to unstimulated controls and expressed as fold change. Events were pregated on leukocytes/singlets/CD11b$^+$CD11c$^+$/live cells. c,d) Productions of IFNβ and IL-1β cytokines by BMDCs after different stimulations. Supernatants of the BMDC culture were harvested 24 h after stimulation for ELISA. e) Percentages of live (Ghost Dye$^-$ Annexin V$^-$) and dead (Ghost Dye$^+$ Annexin V$^+$) cells, pregated as in a. Data are presented as mean +/- s.e.m. $n = 3$ or more independent experiments. Statistical analysis was performed using one-way analysis of variance (one-way-ANOVA). *$p < 0.05$, **$p < 0.005$, ***$p < 0.0005$, ****$p < 0.00005$.

To confirm that the productions of these cytokines are independent, we correlated the BMDC cell death and production of type I IFN and IL-1β. The mean expressions of CD40 expression began to increase within 30 min of exposure to GC; CD86 and MHC-II increased between 10 and 16 h. (Figure S2a,b, Supporting Information). BMDC cell death began between 10 and 16 h after GC simulation (Figure S2c, Supporting Information). IFNβ production began between 6 and 10 h, prior to the initiation of BMDC cell death and activation (Figure S2c,d, Supporting Information). This correlates with the fact that low doses of GC can induce type I IFN but not cell death, confirming that cell death is not required for type I IFN production (Figure 2a–d). Interestingly, the production of IL-1β began 16 h after GC stimulation (Figure S2d, Supporting Information), demonstrating that BMDC cell death and the upregulation of CD86 and MHC-II were correlated with the production of IL-1β (Figure S2c,d, Supporting Information). This time course revealed interesting kinetics between the production of type I IFN and IL-1β, induced by GC, which warrants further investigation.

2.3. GC Induces Proinflammatory Cell Death to Drive Cytokine Production and BMDC Activation

To understand the correlation between the GC-mediated BMDC death and activation, as well as IL-1β cytokine production, we explored different inflammatory cell death pathways.[19] We first investigated pyroptosis, which results from caspase-1/11 cleavage of a pore-forming protein gasdermin D,[20] since the activation of caspase-1 also initiates the cleavage and release of IL-1β.[21] To determine if GC induced pyroptosis through caspase-1 cleavage, we pre-incubated BMDCs with a caspase-1 inhibitor VX765. VX765 did not affect IFNβ production, but inhibited IL-1β cleavage (**Figure 3**a), as expected. Interestingly, VX765 did not inhibit GC-mediated cell death (Figure 3b and c), suggesting that the death of BMDCs does not result from caspase-1 activation. Since caspase-11 can also activate gasdermin D and drive pyroptosis,[22] we measured the gasdermin D levels and found they were significantly reduced by VX765 (Figure 3d), suggesting that caspase-1, not caspase-11, predominantly drives gasdermin D activation in response to GC. These results reveal that GC-mediated BMDC death was not caused by gasdermin D-mediated pyroptosis. Furthermore, BMDC activation is unaltered in the presence of VX765 (Figure 3e), suggesting that caspase-1 cleavage is not required for GC-induced BMDC activation.

Since necroptosis is another important form of proinflammatory cell death triggered through the phosphorylation of RIPK3 and MLKL,[23] we investigated whether necroptosis was involved in GC-mediated cell death. BMDCs were pretreated with a RIPK3 phosphorylation inhibitor GSK'872 before GC stimulation. Little to no changes occurred in cell death, activation, or cytokine production in BMDCs (Figure S3, Supporting Information), implying that necroptosis is not responsible for GC-mediated BMDC cell death.

To further understand GC-mediated BMDC death, live cell imaging was performed using the mouse DC cell line DC2.4, which behaved similarly to BMDCs in many areas such as cell morphology, the expression of dendritic cell-specific markers, the ability to phagocytose, and present exogenous antigens on both MHC class I and class II molecules.[24] After stimulation with FITC-labeled GC for 4–6 hours, we noticed that certain numbers of DCs interacting directly with GC and their neighboring DCs underwent dramatic cellular swelling and eventual rupture, leading either to DC cell death and/or activation of the surrounding DCs (Movie S1, Supporting Information). These results suggest a GC-induced inflammatory cell death, distinct from the traditional necroptotic and pyroptotic pathways.

2.4. STING is Required for Inflammatory Lysosome-Dependent Cell Death and Cytokine Production in GC-Stimulated BMDCs

Since the STING pathway has been shown to play a critical role in innate immune system activation for antitumor activities,[25] particularly as a critical upstream event to produce type I IFN by chitosan,[3] we examined the impact of STING on GC-initiated type I IFN production using the STING "golden ticket" mice.[26] We stimulated BMDCs from wild-type (WT) and Tmem173$^{-/-}$ (STING deficient) mice with GC. IFNα/β production was completely abrogated in the Tmem173$^{-/-}$ BMDCs with or without GC stimulation (**Figure 4**a), indicating STING is required for type I IFN production. Interestingly, IL-1β production is also blocked in the Tmem173$^{-/-}$ BMDCs with GC stimulation (Figure 4b). The mean expressions of CD86 and MHC-II were reduced in Tmem173$^{-/-}$ BMDCs compared to wild type (Figure S4a, Supporting Information), while the mean CD40 expression was not significantly affected (Figure S4a, Supporting Information). Interestingly, cell death in response to GC was also dramatically reduced in Tmem173$^{-/-}$ BMDCs compared to wild type (Figure 4c), suggesting that STING is also required for GC-mediated dendritic cell death.

Since STING has been shown to traffic to the lysosome and initiate lysosome rupture for type I IFN and IL-1β cytokine production[27] and chitosan has been suggested to permeate lysosomal for the similar effect,[14] both being without a clear mechanism, we decided to determine the role of lysosome in GC-mediated cell death and cytokine production. BMDCs were pre-incubated with the lysosomal vacuolar-type H(+)-ATPase inhibitor Bafilomycin A (Baf. A). Baf A dramatically inhibited the production of type I IFN, IL-1β, and gasdermin D (Figure 4d and e), and significantly reduced GC-mediated BMDC cell death (Figure 4f), to the level of that without GC stimulation. Additionally, the mean expression of cell surface activation markers mimicked that observed on unstimulated Baf. A treated BMDCs (Figure S4b, Supporting Information). Collectively, these results indicate that the lysosomes play a key role in GC-mediated cell death, BMDC activation, and cytokine production. Moreover, the results with Baf. A treatment mimicked that observed in the Tmem173$^{-/-}$ BMDCs (Figure 4a–c versus d–f).

Additionally, western blotting (WB) was utilized to illustrate the effects of GC stimulation on STING activation (Figure S4c, Supporting Information). This technique enabled the detection of both the location and relative expression levels of STING. WB was performed on BMDC lysates. Different subcellular components of BMDCs were prepared using a subcellular fractionation protocol. STING was detected within the membrane and lysosomal fractions, with bands observed at ≈35 and 70 kDa, respectively. GC-stimulated BMDCs showed increased STING

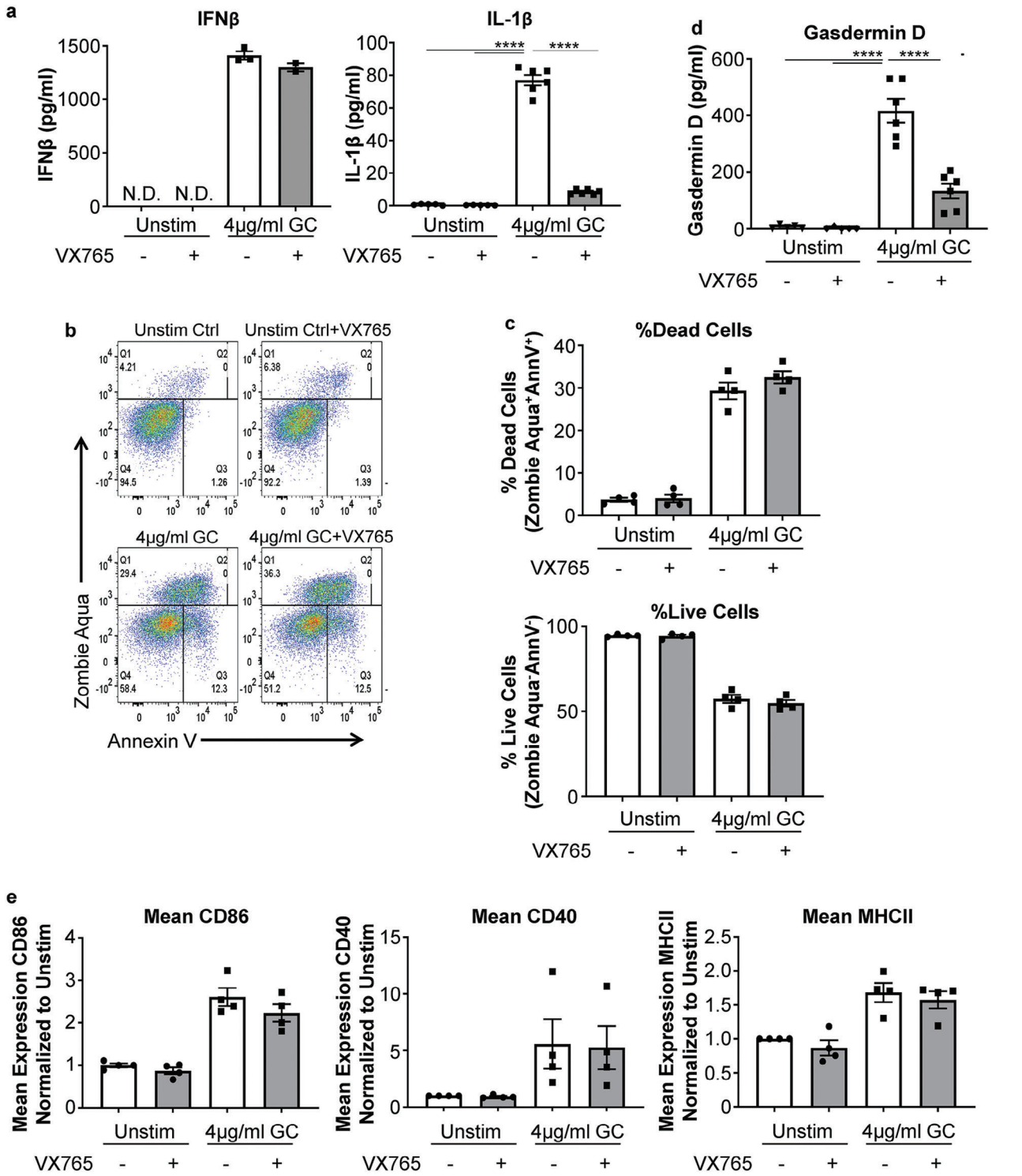

Figure 3. GC drives inflammatory cell death of mouse BMDCs independent of caspase-1 mediated pyroptosis. Mouse BMDCs were pretreated with caspase-1 inhibitor VX-765 for 45 min prior to the addition of GC. Cells and supernatants were collected after 24 h. a) Production of IFNβ and IL-1β by BMDCs after GC stimulation for 24 h. The culture supernatant was used for ELISA. b) Visualization of GC-mediated cell death using Ghost Dye and Annexin V gating. Events were pregated on leukocytes/singlets/CD11b$^+$CD11c$^+$ cells. c) Percentage of live (Ghost Dye$^-$ Annexin V$^-$) and dead (Ghost Dye$^+$ Annexin V$^+$) cells, pregated on leukocytes/singlets/CD11b$^+$CD11c$^+$ cells. d) Expression of Gasdermin D in BMDCs after GC stimulation for 24 h. Cell culture supernatants were used for ELISA. e) Mean expressions of CD86, CD40, and MHC-II, normalized to unstimulated controls and expressed as fold change. Events were pregated on leukocytes/singlets/CD11b$^+$CD11c$^+$/Live cells. Data are graphed as mean +/- s.e.m $n = 3$ or more independent experiments. Statistical analysis was performed using one-way analysis of variance (one-way-ANOVA). *$p < 0.05$, **$p < 0.005$, ***$p < 0.0005$, ****$p < 0.00005$.

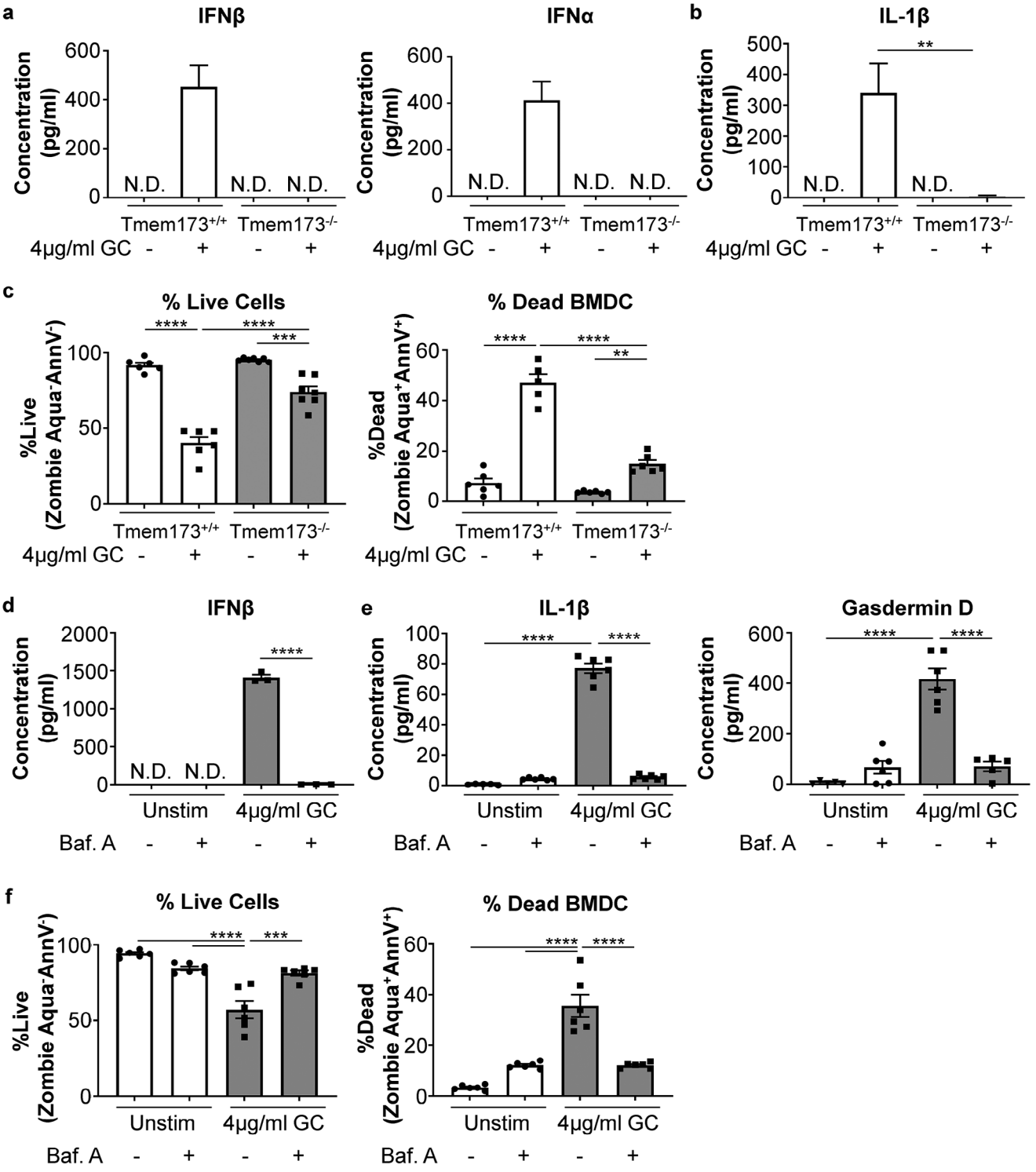

Figure 4. STING and the lysosome are both required for GC to initiate cytokine production and BMDC death. Wild-type and Tmem173$^{-/-}$ (STING-deficient) BMDCs were stimulated with GC for 24 h prior to the collection of the supernatants for ELISA and cells for flow cytometry. a,b) Production of IFNβ, IFNα, and IL-1β by BMDCs after GC stimulation for 24 h. The cell culture supernatants were used for ELISA. c) Percentages of live (Ghost Dye$^-$ Annexin V$^-$) and dead (Ghost Dye$^+$ Annexin V$^+$) cells, pregated on leukocytes/singlets/CD11b$^+$CD11c$^+$ cells. d,e) Production of IFNβ, IL-1β, and Gasdermin D cytokines by BMDCs, pretreated with lysosomal inhibitor Bafilomycin A for 45 min, followed by GC stimulation for 24 h. Cells and supernatants were collected after 24 h. Supernatants were used for ELISA and cells for flow cytometry. f) Percentages of live (Ghost Dye$^-$ Annexin V$^-$) and dead (Ghost Dye$^+$ Annexin V$^+$) cells, pregated on leukocytes/singlets/CD11b$^+$CD11c$^+$ cells. Data are presented as mean +/- s.e.m. $n = 3$ or more independent experiments. Statistical analysis was performed using one-way analysis of variance (one-way-ANOVA). *$p < 0.05$, **$p < 0.005$, ***$p < 0.0005$, ****$p < 0.00005$.

levels, especially in the lysosome. The bands also suggested STING dimerization in the lysosome upon GC stimulation, as the protein dimerizes once activated. These findings confirmed an uptake in STING activation and its trafficking to the lysosome in response to GC stimulation.

This suggests that the interaction between STING and lysosomes is the likely cause of lysosomal-mediated cell death, induced by GC, to activate the immune response similarly as described in human monocytes.[28]

2.5. GC Induces Robust Type I IFN Antitumoral and Antiviral Responses in BMDCs through Cellular Death

To further investigate the roles of STING in mediating GC-induced cellular responses, we followed the orthogonal experimental design of a two-conditions (without and with GC treatment) and two-genotypes (WT and Tmem173$^{-/-}$), with interaction terms[29] (Figure S5a, Supporting Information), to perform bulk RNA sequencing (RNAseq) for BMDCs.

Using the mRNA of protein-coding genes, we generated heatmaps of sample-to-sample distances using the variance stabilizing transformation (vsd) values (**Figure 5a**). Figure 5a showed that the largest distance existed between the WT BMDCs with and without GC stimulation, suggesting that GC induced broad transcriptional profile changes. Meanwhile, the distance between unstimulated WT and Tmem173$^{-/-}$ BMDCs is the smallest, indicating that they both had similar gene expressions without GC stimulation. The responses of GC-stimulated Tmem173$^{-/-}$ BMDCs were remarkably similar to that of unstimulated wild type and Tmem173$^{-/-}$ BMDCs, but significantly different from that of GC-stimulated WT BMDCs. This suggests that STING may play a crucial role in mediating GC activation of BMDCs. We also conducted the differentially expressed genes (DEGs) analysis by comparing transcriptional profiles in GC-treated WT BMDCs versus untreated BMDCs. Expressions of these GC-triggered DEGs shown by the heatmap indicated that GC-promoting genes (upregulated DEGs) and GC-inhibiting genes (downregulated DEGs) contain both STING-dependent and STING-independent transcriptional signatures (Figure S5b, Supporting Information).

Next, we dissected the STING-dependent, GC-promoting, and GC-inhibiting transcriptional profiles by using *DESeq2* package[30] following the two-factor analysis and visualized in the heatmap and a volcano plot (Figure 5b and c). The STING-dependent, GC-induced DEGs contained both downregulated and upregulated expression patterns when compared to WT BMDCs with GC treatment, corresponding to GC-promoting genes (Figure 5c, left) and GC-inhibitory genes (Figure 5c, right). As expected, the top GC-promoting genes in WT were *interferon beta* (*Ifnb1*) and type I IFN response genes (Figure 5c, left) consistent with the observation using cytokine ELISAs for the proteins produced (Figure 4a). STING-dependent, GC-promoting genes are shown in Table S1 (Supporting Information). STING-dependent, GC-inhibitory genes were shown in Table S2 (Supporting Information).

Our Gene Ontology (GO)[31] enrichment analysis also showed that STING-dependent, GC-promoting genes were enriched in biological processes including responses to virus and IFNβ/g (Figure 5d). This was further confirmed by our Kyoto Encyclopedia of Genes and Genomes (KEGG)[32] enrichment analysis, which showed the involvement of pathways including infection, virus, Toll-like receptor (TLR), antigen processing and presentation, necroptosis, RIG-I-like receptor (RLR), and TNF signaling (Figure S5c, Supporting Information). On the other hand, the STING-dependent, GC-inhibitory genes were enriched in the biological processes and pathways of cell cycle and cell nuclear division (Figure S5d, Supporting Information). For example, expressions of cell cycle-related genes, including *Ccnb1*, *Top2a*, *E2f7*, *Cdc25c*, and *Mki67*, were significantly downregulated in GC-stimulated WT BMDCs. However, this STING-dependent GC-inhibition was attenuated in Tmem173$^{-/-}$ BMDCs (Figure 5e; Figure S5e, Supporting Information). These results support our previous observation that GC treatment led to STING-dependent cell survival/cycle reduction and cell death augmentation (Figure 4c).

2.6. GC Requires STING to Activate BMDCs and to Promote the Activation of a Variety of Nucleic Acid Pattern Recognition Receptors

To further explore the antitumor and antiviral response pathways activated by GC, we focused on positive and negative regulators of the nucleic acid sensing pattern recognition receptors (PRRs), such as STING, MAVS/RIG-I, TLR3, and TLR7/9 (Figure 5e; Figure S6a–c, Supporting Information). As expected, the unstimulated samples, regardless of genotype, were nearly identical in their gene expression patterns (Figure 5e). Furthermore, the genes expressed in the GC-stimulated Tmem173$^{-/-}$ BMDCs were like the unstimulated controls, confirming that STING pathway genes were not activated by GC in its knockout genetic background (Figure 5e).

In addition, STING signaling can activate TBK1/IRF3 or TBK1/IRF7 signaling pathways and/or canonical and noncanonical NFkB signaling.[33] Based on gene expression patterns in the WT BMDCs, 24 h after stimulation, GC drove STING signaling preferentially through TBK1/IRF7, but not TBK1/IRF3, in addition to both canonical and noncanonical NFkB signaling (Figure 5e). Next, we examined the expression of upstream mediators of STING activation: cGAS, Zbp1 (also known as DAI), DDX41, and IFI16 (also known as Ifi204). The expressions of cGAS and DDX41 were equivalent between the unstimulated and GC-mediated WT BMDCs but were decreased in GC-stimulated Tmem173$^{-/-}$ BMDCs (Figure 5e). Surprisingly, Zbp1 and Ifi204 are specifically enriched in the GC-stimulated WT BMDCs. Both are cytosolic nucleic acid sensing proteins that signal through STING to initiate type I IFN production. Zbp1 is unique in that it is capable of also binding dsDNA and dsRNA,[34] ribonucleoprotein complexes,[35] and also activating RIPK3, to drive necroptosis.[36] This is complemented by our in vitro data demonstrating that blocking RIPK3 activation slightly reduced GC-mediated BMDC cell death (Figure S3b, Supporting Information). Since Ifi204 is a cytosolic dsDNA sensor that plays a key role in herpes simplex virus type 1 (HSV-1) immunity[37] and it was preferentially induced in response to GC as opposed to cGAS (Figure 5e), our results support our hypothesis that, in contrast to chitosan,[3] GC activation of STING in DCs may be cGAS-independent.

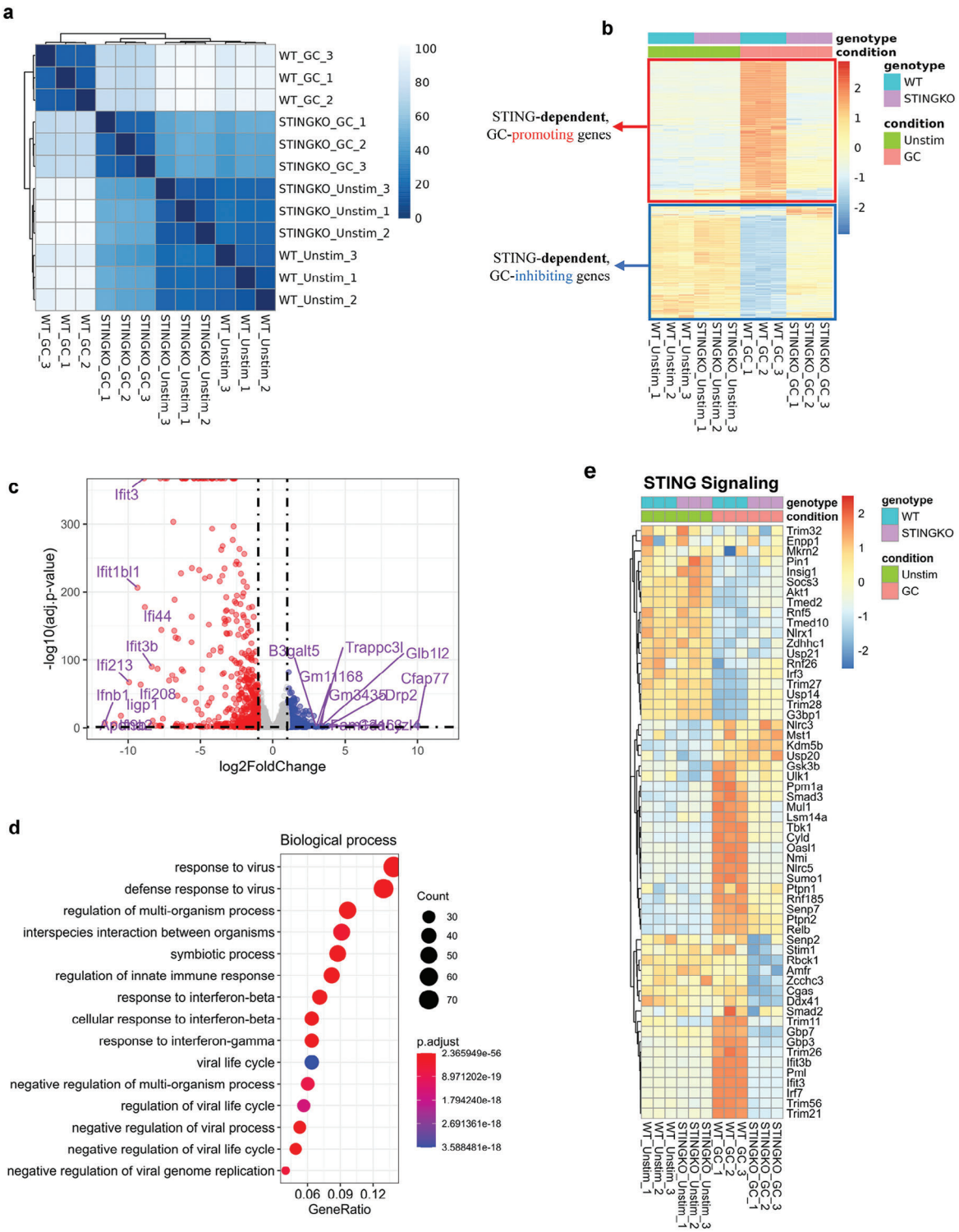

Figure 5. GC is unable to activate BMDCs in the absence of STING. Wild-type (WT) and STING-deficient (Tmem173$^{-/-}$) BMDCs were stimulated with GC for 24 h prior to collection. Cells were sorted on Live/CD11b^{+}CD11c^{+} BMDCs prior to total RNA isolation. a) Heatmap of sample-to-sample distances using the variance stabilizing transformation (vsd) values of mRNA expression of protein-coding genes. b) Heatmap schematically showing the STING-dependent GC-promoting genes (in red box) and GC-inhibiting genes (in blue box). Each row represents a gene (gene name not shown). c) Volcano plot demonstrating the expressions of STING-dependent, GC-promoting genes (red color) and GC-inhibiting genes (blue color). Each dot represents a STING-dependent gene. d) Dot plot demonstrating the enrichment analysis for STING-dependent GC-promoting genes using biological process (BP) of gene ontology (GO) database. e) Heatmap showing the expressions of STING pathway genes in WT and Tmem173$^{-/-}$ BMDCs with and without GC treatment. Wild-type and STING-deficient (Tmem173$^{-/-}$) BMDCs were stimulated with GC for 24 h prior to collection.

Since it has been suggested that chitosan is a mitochondrial toxin and that the production of ROS and the release of mitochondrial DNA/RNA activate an immune response,[3] and in that case, other nucleic acid PRRs and the NLRP3 inflammasome should still be activated even in the absence of STING, we generated heatmaps of genes involved in several PRRs including RIG-I/MDA-5, TLR-3, −7, and −9 signaling. The results revealed that these pathways were only activated in the GC-mediated WT BMDCs, not in the Tmem173$^{-/-}$ or unstimulated BMDCs (Figure S6a–c, Supporting Information). This suggests that mitochondrial function was not directly affected by GC. Moreover, these data showed that the activation of RIG-I/MDA-5, and TLR-3, −7, and −9 signaling pathways were downstream of STING. The activation of these pathways is consistent with the notion that GC is mediating a form of pro-inflammatory cell death, specifically through STING, to activate neighboring BMDCs through a variety of nucleic acid sensing pathways. This unique method of DC activation, combined with the fact that GC upregulates a variety of antiviral responses, suggests that GC could function as a broadly effective antitumor immunostimulant or antiviral vaccine immunoadjuvant.

When WT BMDCs were compared to the Tmem173$^{-/-}$ BMDCs upon GC stimulation, no stress response genes were upregulated in the GC-mediated Tmem173$^{-/-}$ BMDCs, indicating that GC was not a direct mitochondrial toxin and/or it did not result in direct lysosomal leakage, as genes for lysophagy and mitophagy were not upregulated in the absence of STING compared to WT BMDCs (Figure S7a,b, Supporting Information).

2.7. Intratumoral Injection of GC Drives a Type I IFN, Proinflammatory Tumor Microenvironment

To determine how GC exerts its effects on myeloid cells in vivo, we injected MMTV-PyMT tumors with GC, isolated the tumor-infiltrating immune cells, and performed single-cell RNA-Sequencing (scRNAseq) as previously described.[13b] To explore the heterogeneity of the myeloid cells, we used shared-nearest neighbor (SNN) to cluster the myeloid cells. Using principal component analysis (PCA), we obtained 12 clusters (C0-C12), annotated using a series of commonly used immune cell genes (**Figure 6a**; Figure S8a, Supporting Information).

For macrophage clusters, C1 was enriched with interferon genes Ifi208, Ifitm3, and ISG15. C7, C8, C10 were all cycling macrophages, highly expressed with E2f1, Mki67, and Top2a. C4 was annotated as Tgfb^{+} Mac due to specific and high expression of Tgfb3, Aldoa, and Vegfa. C5 showed the highest expressions of Apoe and C1qa. It is worth noting that C2 showed the phenotypes of both granulocytic monocyte-derived suppressor cells (G-MDSCs) and neutrophils due to expressions of G-MDSC markers Cd84, Il1b, Spi1, Asprv1, Plscr1, Pirb and neutrophil markers Fcgr3, Sirpb1c, Clec4d, Cd14, Lcn2. However, this cluster did not express another set of neutrophil markers Elane, Mpo, Prtn3, Camp, Ltf, Ly6g (Gr1). Therefore, C2 was named G-MDSC but with certain non-immune suppressive property due to the lack of expression of Arg1(Arginase 1) and Tgfb1.

The proportions of immune cells in the 12 clusters were compared between the untreated and GC-mediated cells (Figure 6b). GC enhanced the proportions of G-MDSCs (C2, +281%), monocytes (C9, +50%), macrophages (C1, +107%), plasmacytoid DCs (pDCs, C6, +53.1%), and conventional DCs (C11 and C12, +77.6% and +54.3, respectively). Conversely, GC decreased the proportion of select macrophages (C0, −53.6%; C4, −143%; C5, −12.9%; C7, −73.4%; C8, −87.4%; and C10, −71.4%), within the TME (Figure 6b; Figure S8b, Supporting Information).

Since STING can interact with *Tbk1, Ikbkg*, and *Traf6* to drive type I IFN production, and canonical or noncanonical NFkB signaling,[33a,c,37] we examined several genes involved in STING signaling cascades and discovered the most significant upregulation of genes occurred in the monocytes and the three DC clusters (Figure 6c). Monocytes with upregulated expressions of *Tbk1, Ikbke (IKKε), Irf3 Ikbkg (NEMO), Ikbkb (IKKβ), Chuk (IKKα)*, and *Nfkb1 (p50)* correspond to the conventional STING signaling, type I IFN production, and the activation of canonical NFkB signaling gene targets.[33a] A similar pattern was observed in cDCs (C12), and pDCs (C6). In C11, cDCs with upregulated *Tbk1, Nfkb1, Irf7*, and *Irf3*, suggest conventional STING signaling. Interestingly, cells in C11 also have upregulated genes *Nfkb2* and *Relb*, both involved in noncanonical NFkB signaling.[33c] These results indicate that STING signaling is in fact occurring in the monocytes and DC subtypes in response to GC, corroborating our in vitro findings using BMDCs.

We next examined the expression of cytokines, chemokines, and regulatory molecules in all the myeloid cell subsets. Interestingly, the monocytes and pDCs did not express proinflammatory cytokines while cDC expressed upregulated proinflammatory cytokines and chemokines (Figure S8c, Supporting Information). This is significant for CD8^{+}T cell activation in the TME as DCs play a major role in activating and cross-priming T cells in the TME.[13a,38] Of significant importance, an increase in CD8^{+} T cells is associated with improved patient outcomes.[39] Examining the macrophage clusters more closely revealed that the only macrophage cluster that increased in numbers, C1 (Figure 6b), has the upregulated expressions of *Cd40, Il1b, Cxcl10, Tgm2*, and *Nos2*, and molecules and cytokines associated with inflammation and T cell activation (Figure S8c, Supporting Information). The other macrophage subsets, which decreased in number with the addition of GC, exhibited increases in anti-inflammatory and negative immune regulating molecules, such as *Il10, Tgfb, Arg1, Vegfa, Apoe*, and *Socs3*, to various degrees (Figure S8c, Supporting Information). These results suggest that the macrophages in C1 exhibit a more proinflammatory phenotype, which helps control tumor growth, while the remaining macrophage clusters are more anti-inflammatory.

To further explore the proinflammatory (M1-like) and anti-inflammatory (M2-like) macrophage phenotypes present in the TME, we used a scatter plot to compare traditional M1- and M2-like gene expression patterns for untreated control cells (shown in red in Figure 6d) and GC-treated cells (shown in turquoise in Figure 6d). Macrophages in clusters 0, 4, 5, 7, 8, and 10 revealed a similar M2-like protumor signature between the untreated and GC-treated cells, albeit there were fewer numbers in the GC-treated group (Figure 6d). Interestingly, the macrophages in C1 demonstrated that a portion of cells with upregulated genes associated with M1-like macrophages, suggesting that these cells are more inflammatory or anti-tumor (Figure 6d). More importantly, the macrophages that shifted toward the M1-like phenotype were almost exclusively from the GC-treated tumors. This

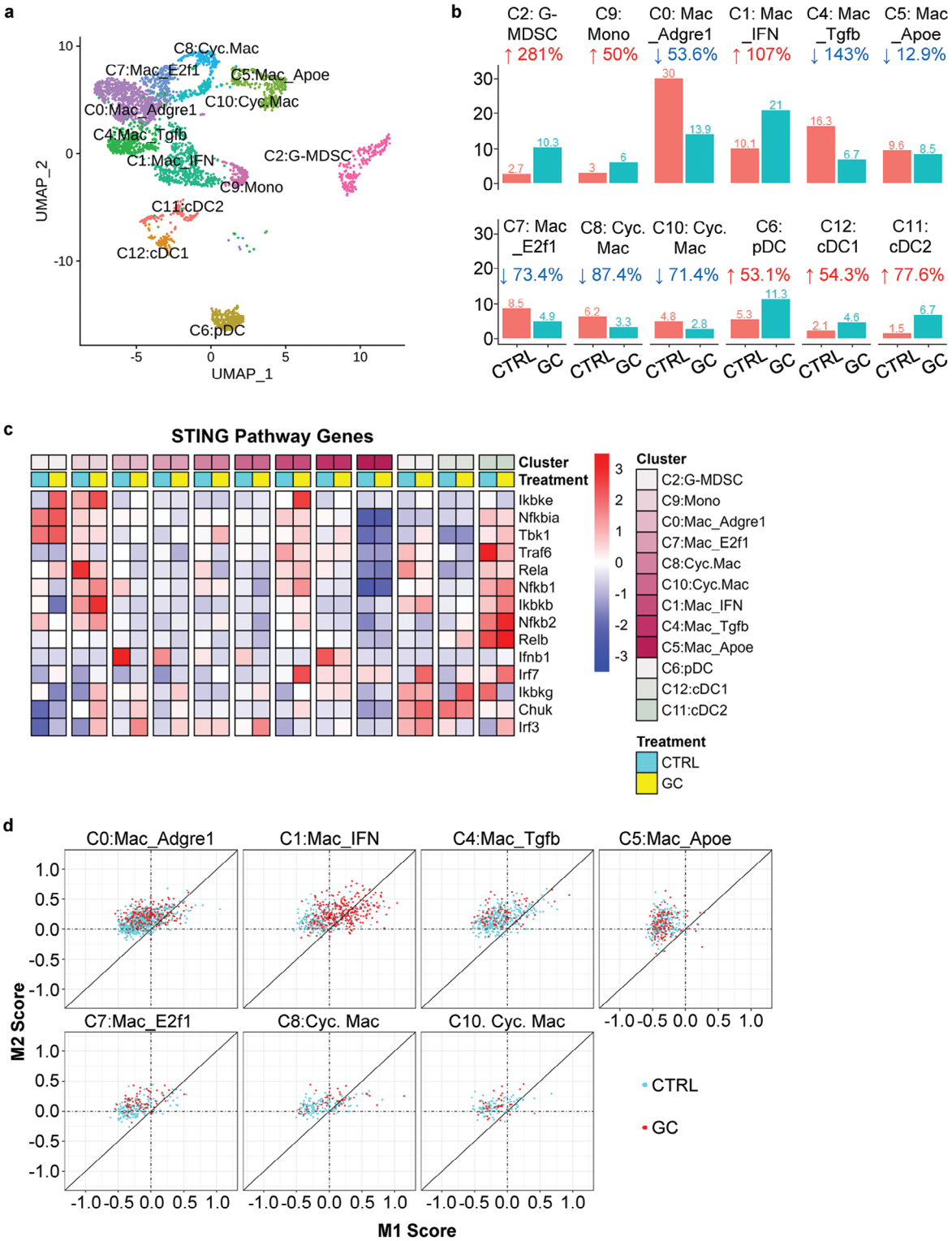

Figure 6. GC remodels myeloid cell proportions/heterogeneity and activation status in the tumor microenvironment. Wild-type FVB females were injected with MMTV-PyMT tumor cells directly into the mammary tissue. Once the tumors reached ≈0.5 cm^3, animals were either left untreated or injected with 1% GC (0.1 ml). Tumors were collected 10 days post-treatment, and tumor-infiltrating $CD45^+$ cells were purified and used for single-cell RNA sequencing. a) UMAP of myeloid cell subtypes, including monocyte, macrophage (Mac), dendritic cell (DC), and myeloid-derived suppressing cell (MDSC). b) Bar plots displaying the proportions of myeloid cells from untreated (CTRL) and GC-treated tumors. Percentage change from CTRL to GC was displayed. c) Heatmap highlighting expression of genes involved in the STING signaling pathway. d) Scatter plots highlighting the macrophage clusters and their M1- and M2-like macrophage scores.

corresponds well with the activation signature observed in the GC-treated macrophages in C1 (Figure S8c, Supporting Information). Although our analysis indicated that cluster C1 predominantly contains macrophages exhibiting an M1-like phenotype, and the remaining clusters are characterized by cells with M2-like phenotypes, further investigation is required to accurately determine the specific identities of these cell subtypes. As shown in Figure 6, GC significantly reduced the numbers of M2-like macrophages, likely through inflammatory cell death similar to GC-mediated DC death.

Since it is known that tumor-associated macrophages (TAMs) are indicators of treatment resistance, tumor progression, and metastases,[40] GC's reductive effect on M2-like macrophages (Figure 6a–d) could play a significant role in the treatment of metastatic cancers, particularly when combined with a localized tumor ablation.[8,9,11–13]

3. Discussion and Conclusion

In the current work, we investigated the cellular and molecular mechanisms by which GC activates strong antitumor and antiviral immune responses. First, we discovered that GC could not directly activate non-phagocytic cells such as T cells or kill tumor cells (data not shown), consistent with the previous results using chitosan for the activation of APCs.[14] Instead, GC must be actively engulfed to activate APCs such as monocytes, macrophages, and DCs. Work by others also suggested that, following phagocytosis, chitosan triggers lysosomal leakage, leading to the activation of the NLRP3 inflammasome/pyroptosis pathway and mitochondrial stress, resulting in the activation of the cGAS/STING pathway to produce type I IFNs.[3,14] These studies concluded that chitosan was passive in inducing the immune response and that immune stimulation occurred via lysosomal leakage-induced cellular stress.

We synthesized *N*-dihydrogalactochitosan (GC) to create a new molecule that is both more soluble and significantly more potent than its corresponding chitosan, allowing it to become a viable drug candidate for clinical use. Using human THP-1 cells, which resemble monocytes and macrophages in morphology and differentiation properties, we showed that GC was much more effective than chitosan in inducing type I IFN production and activation (Figure 1). We also found that GC-induced cell death correlates with IL-1β production (Figure 2). We determined that GC did not induce pyroptosis (Figure 3c); instead, it initiated STING-dependent lysosomal cell death (Figure 4c). Without the critical cytosolic sensor STING, BMDC death was drastically reduced, and type I IFNs and IL-1β were completely abrogated (Figure 4a and b). Furthermore, we ascertained that the lysosome played a key role in GC-initiated production of type I IFN and IL-1β (Figure 4d). Western blot results demonstrated increased STING expression levels in GC-stimulated BMDCs, with the lysosomal isolates displaying larger and more intense STING expression bands in the stimulated group compared to the control group. This increased expression within BMDC lysates indicated that GC interacts with the STING signaling pathway, resulting in STING trafficking for further downstream processing and cellular responses.

In human monocytes, it has been reported that in certain viral infections, cGAS activation of STING can cause STING trafficking to the lysosome via an unknown mechanism and it initiates lysosomal rupture to activate the NLRP3 inflammasome.[28] The mechanism of GC appears to be similar, but the involvement of cGAS was not clear. We compared the activation of WT and Tmem173$^{-/-}$ BMDCs following GC stimulation and found that Tmem173$^{-/-}$ BMDCs stimulated with GC were similar to the unstimulated controls (Figure 4). The results in Figure 4 indicate that STING is required for DC activation and GC was not a mitochondrial toxin; it did not cause significant amounts of lysosomal leakage in the absence of STING. Furthermore, Tmem173$^{-/-}$ BMDCs stimulated with GC did not elevate genes involved in mitochondrial or lysosomal stress (Figure S7, Supporting Information), suggesting that GC plays an active role in stimulating STING and that STING is directly required for GC-mediated activation and lysosomal leakage. This is corroborated by the fact that cGAS expression is not upregulated in response to GC (Figure 5e). It should be noted that other STING-activating molecules, such as Zbp1 and IFI16 (Ifi204), were highly enriched by GC (Figure 5e). Whether these molecules are required for GC-mediated STING activation requires further investigation.

It has recently been demonstrated that STING can be activated by a polyvalent polymer containing a seven-membered ring with a tertiary amine (PC7A).[41] This molecule does not bind STING at the same site as the cyclic dinucleotides like 2′3-cGAMP, and this alternate binding to STING prolongs the type I IFN response compared to cyclic dinucleotides.[41] Furthermore, it was found that cGAMP initiated a strong immune response within the first couple of hours, peaking at 6 h, while PC7A initiated a peak stimulation between 24 and 48 h, effectively sustaining the STING activation.[41] Our kinetic studies with GC revealed that type I IFN production did not begin until ≈10 h after stimulation and continued to increase over a 24 h period (Figure S2d, Supporting Information). This suggests that GC may act similarly to PC7A in sustaining STING signaling. However, the advantage of GC, compared to PC7A, is its capability to drive alternative activation of STING, resulting in an inflammatory cell death that further enhances APC recruitment and activation through a variety of pattern recognition receptors (PRRs), such as toll-like receptors (TLR), nucleotide-binding and oligomerization domain (NOD)-like receptors (NLRs), and retinoic acid-inducible gene I (RIG-I)-like receptors (RLRs), as shown in Figure S6 (Supporting Information).

Our analysis of the myeloid cells isolated from GC-injected MMTV-PyMT tumors revealed a STING activation signature in cDCs and a dramatic shift in the macrophage populations toward inflammatory macrophages (Figure 6b and c). Furthermore, GC increased the proportions of DCs, while simultaneously decreasing the anti-inflammatory macrophages residing within the TME (Figure 6b and d). Our results showed an increase in the G-MDSC population after GC stimulation. G-MDSC is a heterogeneous cell population and while traditionally thought to be immunosuppressive, some studies showed that neutrophilic cells in this population can activate CD8$^+$ T cells, following activation by interferon.[42] In our previous study, the high levels of neutrophils have been associated with GC-induced anti-tumor response.[43] Therefore, the effects of the increased G-MDSC by GC in our study were not clear in immune suppression, and further studies are needed. One might wonder if MDSCs counteract the immune stimulation by GC. G-MDSC-like cells were

observed in this genetic analysis, but their function and activities remain to be verified by ex vivo assays. This observation may indicate the beginning of a wound-healing process after ablation. The kinetics of infiltration of granulocytic cells, inflammatory M1-like macrophages, and activated DCs within the tumor microenvironment need to be elucidated with further studies. These results indicate that GC is a strong type I IFN stimulant that can alter the TME, making it more inflammatory which precedes immune-mediated tumor killing.

We hypothesize that different immune cells respond to GC in various ways, involving distinct pathways. The macrophage-induced immune response may further activate DCs. DCs can be activated via multiple pathways, both directly by GC and indirectly by other immune cells. We are conducting further studies to determine GC-induced type I IFN responses in macrophages, the timing of activation, the cross-talk between different immune cells, and the pathways of type I/II IFN stimulation by GC.

In summary, GC triggered conventional and alternative activations of STING to synergize type I IFN and IL-1β production. GC also triggers the activation of PRR with pathways leading to enhanced antigen processing and presentation as well as cytokine production, all leading to enhanced tumor killing involving CD8+ T cells. These novel functions and the unique mechanism by which GC activates phagocytic cells make it a promising therapeutic immunostimulant for generating broad innate and adaptive antitumor and antiviral responses.

4. Experimental Section

GC and Chitosan: *N*-dihydrogalactochitosan (GC) and chitosan was provided by Immunophotonics, Inc. (St. Louis, MO). GC was synthesized, purified, characterized, and tested for impurities under GMP conditions, and the same batch of GC was used in all experiments. The chitosan used for experiments shown in Figure 1 and Figure S1 (Supporting Information) was from the same batch of chitosan that was used as starting material in the synthesis of the GC. Additionally, the chitosan was processed and purified under identical conditions as the GC (except for the synthetic steps) and was characterized and tested to ensure that the chitosan and GC materials were identical, except for the galactose moieties on the GC molecule (Figure S9, Supporting Information). The synthesis process of GC was described briefly below.

An appropriately sized glass-lined vessel, equipped with a cooling jacket and overhead stirring was charged with 8% aqueous acetic acid (130 g). The resulting solution was stirred and charged with chitosan (2.33 g, 13.71 mmol) followed by D-galactose (12.53 g, 69.58 mmol). The resulting suspension was charged with additional 8% aqueous acetic acid (100 g) and stirred vigorously at ambient temperature for a minimum of 12 h. The resulting solution was cooled to 6–8 °C using jacketed cooling then diluted with water (167 g). The pH of the solution was adjusted to a value of 4 using a 2.0 M aqueous solution of sodium hydroxide (added in 2.4 mL aliquots until the desired pH was achieved). The resulting solution was then dosed with a 0.91 M solution of sodium borohydride in 4.72 mM aqueous sodium hydroxide over a period of 6.5–7 h using a calibrated dosing pump. The borohydride solution was added in a subsurface manner, via 2 subsurface addition ports. Gas evolution and foaming was observed throughout the titration and the stirring speed was adjusted to ensure the foaming did not exceed the height of the cooling jacket. The reaction was monitored for pH and temperature during the entire borohydride titration, with the pH being adjusted with glacial acetic acid (in 2.7 mL aliquots) when the pH reached 4.5 and the cooling adjusted based on the temperature read via a subsurface thermowell. Upon completion of the sodium borohydride titration, the resulting solution was allowed to warm to ambient temperature overnight with reduced stirring. The resulting solution was then purified by diafiltration using a 30 kDa cutoff hollow fiber filter (6 passes). The resulting solution was ultrafiltered to a volume of ≈0.4 L, then passed through a 0.22-micron cartridge filter into a sterile biobag. The resulting solution was subjected to assay testing by HPLC to determine the concentration, then further diluted with water or ultrafiltered to obtain a final solution of GC with a concentration of 10 mg mL^{-1}. The resulting solution was analyzed, and the results are summarized in Figure S9 (Supporting Information).

Bone Marrow-Derived Dendritic Cell Cultures: Bone marrow was isolated from 8 to 12-week-old male or female mice. Briefly, the animals were euthanized according to IACUC-approved protocols. The hind legs were removed and separated from the muscles and sinew. The heads of the bones were removed and 1x PBS was pushed through the bones using a 25-gauge needle and a 1 ml syringe. The red blood cells were lysed, and cells were resuspended in RPMI containing 20% heat-inactivated fetal calf serum, pen/strep, and β-mercaptoethanol. About 5 × 10^6 bone marrow cells were plated into 100 mm non-tissue culture-treated plates containing 20 ng ml^{-1} granulocyte-macrophage colony-stimulating factor (GM-CSF) (Biolegend, Cat# 640 920). On day 3 5 ml of fresh media containing 20 ng ml^{-1} of GM-CSF was added to the cultures. On day 6 non-adherent cells were collected, and the medium was removed and replaced with fresh RPMI containing 20 ng ml^{-1} GM-CSF and placed back into the 100 mm plate. On day 7 the nonadherent BMDCs were collected for stimulation.

BMDC Activation: BMDCs were stimulated with GC or 2′3-cGAMP (InvivoGen, Cat# tlrl-nacga23-1) for 0–24 h prior to ELISA or flow cytometry. About 10^6 cells ml^{-1} BMDCs were plated into a non-tissue culture treated 96 well round bottom plate and then stimulated with 0.08–16 µg ml^{-1} GC. For 2′3-cGAMP stimulation, 200 ng of 2′3-cGAMP was first encapsulated into viromer green transfection reagent (Origene, Cat# TT100301) according to the manufacturer's instructions prior to incubation with BMDCs.

VX765 was purchased from InvivoGen (Cat# inh-vx765i-1) and used at a concentration of 10 µM. BMDCs were pre-incubated for 45 min with VX765 prior to the addition of GC. Bafilomycin A was purchased from InvivoGen (Cat# tlrl-baf1) and used at a concentration of 100 nM. BMDCs were pre-incubated for 45 min with bafilomycin A prior to the addition of GC. GSK'872 was purchased from Millipore Sigma (Cat# 530 389) and used at a concentration of 3 µM. BMDCs were pre-incubated for 45 min with GSK'872 prior to the addition of GC.

RNA-Sequencing: BMDCs were cultured for 24 h, then harvested and stained with ghost dye BV510 for viability and CD11b APC-Cy7 and CD11c FITC. Live CD11b$^+$CD11c$^+$ BMDCs were sorted on the BD FACS ARIA. RNA was isolated from the sorted BMDCs using the Quick-RNA microprep kit purchased from Zymo Research (Cat# R1050). RNA was isolated according to the manufacturer's protocol. For sequencing the 20 M reads mRNA prep and sequencing service was performed for preparation of the RNA for NovaSeq PE150 reads on the NovaSeq6000.

Bioinformatics Analysis (Quality Control, Read Trimming, Mapping to Genome, and Identification of DEGs): A quality check for the raw sequencing data was conducted using *FastQC* (v0.11.9) to detect common issues in RNA-Seq data. The reads were then trimmed with *Trimmomatic* (v0.39) to remove low quality bases.[44] The quality of the reads was re-evaluated with *FastQC* after this step to validate the quality improvements. The RNA-seq reads from each sample were mapped to the mouse mm10 genome assembly using the *HISAT2*. *Samtools* was used to manipulate the *HISAT2* generated SAM files into BAM files.[45] *FeatureCounts* program from *Subread* package was used to count mapped RNAseq reads for genomic features.[46] *DESeq2* was used for differential expressed genes (DEG) analysis based on the negative binomial distribution. The resulting P-values were adjusted using the Benjamini and Hochberg's approach for controlling the false discovery rate. Genes with an adjusted P-value (P adj) < 0.05 as determined by *DESeq2* were assigned as differentially expressed. Gene ontology (GO) analysis of DEG was performed using *clusterProfiler*.[47]

Flow Cytometry of BMDCs: All samples were run on the BD FACSCelesta and data were analyzed using FlowJo v10.6.1. After BMDC stimulation for 0–24 h with GC or 2′3-cGAMP, BMDCs were isolated and stained with the antibodies, CD11c-FITC (Tonbo Bioscience, cat#

35–0114), CD11b-APC-Cy7 (Tonbo Bioscience, Cat# 25–0112), CD40-PE-Cy7 (Biolegend, Cat# 124 622), MHCII-RedFluor710 (Tonbo Biosciences, Cat# 80–5321), CD86-BV605 (Biolegend, Cat# 105 037), Ghost Dye-Violet-510 (Tonbo Biosciences, Cat# 13–0870), and Annexin V-APC (Biolegend, Cat# 640 920). Briefly, cells were stained on ice with all antibodies and viability dye for 20 min. The cells were then washed and resuspended in Annexin V staining buffer for 15 min and then immediately ran on the BD FACSCelesta. Briefly, cells were gated on $CD11c^+CD11b^+$ cells and then assessed for ghost dye BV510 and Annexin V expression. For the mean expression of CD40, CD86, and MHCII, the cells were gated on $CD11c^+CD11b^+$ live cells before analysis. Bar graphs were generated using Graphpad Prism software.

Cytokine ELISA: After BMDC stimulation with GC or 2′3-cGAMP for 0–24 h, BMDCs were isolated and pelleted, and the supernatant was collected and frozen at −80 °C until the ELISAs were performed. The mouse IFNβ and IFNα ELISA kits were purchased from R&D systems (Cat# MIFNB0), mouse IL1β ELISA kits were purchased from ThermoFisher Scientific (Cat# 88-7013-22), and mouse gasdermin D ELISA kits were purchased from IBL America (Cat# IB99570). ELISAs were performed according to manufacturers' instructions. The ELISA plates were read using the Biotek Synergy H1 Hybrid plate reader, and the data were analyzed and graphed using the Graphpad Prism software.

Animals: All animal studies were either approved by the IACUCs of Oklahoma Medical Research Foundation or the University of Oklahoma. C57BL/6, C57BL/6J-*Sting1*^{gt}/J, and FVB mice were purchased from Jackson Laboratories (Stock numbers: 000664, 01 7537, and 0 01800).

Syngeneic Tumor Cell Transplantation: MMTV-PyMT murine breast tumor organoids were isolated from FVB/N-Tg (MMTV-PyVT) 634Mul/J mice as previously described.[48] Briefly, cells were incubated overnight in mammary epithelial cell media (DMEM/F12 supplemented with 10% fetal bovine serum (Sigma–Aldrich, F2442-500ML), 100 U mL^{-1} penicillin-streptomycin (Sigma–Aldrich, P0781-20×100 ml), 5 ug mL^{-1} insulin-transferrin-selenium (ThermoFisher Scientific, 51 500 056), 1 ug mL^{-1} hydrocortisone (Sigma–Aldrich, H0888-10G), 10 ng mL^{-1} mouse epidermal growth factor (EGF) (ThermoFisher Scientific, 53 003 018), and 50 ug mL^{-1} gentamicin (Genesee Scientific, 25–533). Cells were washed twice with Hepes Buffered Saline (HBSS) (Gibco, 14175-095), trypsinized, and resuspended to a concentration of 1×10^5 cells per 20 uL. Cells were injected into the mammary fat pad of wild type FVB mice without clearing. The incision was closed with Vetbond tissue adhesive (3 M). Once the tumors reached 0.5 cm^3 the tumors were either left untreated or injected with 100 µl of 1% GC (Immunophotonics, St. Louis, MO).

Sample Preparation and Single-Cell RNA Sequencing Library Generation: In each of the two treatment groups, immune cells from four mice were used for single-cell RNA sequencing. Nine days after treatment, tumor tissues were isolated, minced with scalpels, and digested with Collagenase IV and DNase I at 37 °C for 20–30 min. After enzymatic digestion, immune cells were enriched using lymphocyte separation medium. The enriched cells were then subjected to magnetic bead separation (EasySep Mouse Streptavidin Rapidspheres Isolation Kit, Stem Cell, 19 860) to remove the $EpCAM^+$ cells (CD326 1:200, ThermoFisher Scientific, 13-5791-82). The EpCAM-depleted cells were stained with antibodies against CD45 and a viability dye. Live $CD45^+$ cells (CD45 1:100, Biolegend, 103 112), were sorted using MoFlo and then processed for droplet-based 3′ end scRNAseq by encapsulating sorted live $CD45^+$ tumor-infiltrating immune cells into droplets via a 10× Genomics platform according to the manufacturer's instructions (10× Genomics). Paired-end RNA-seq was performed via an Illumina NovaSeq 6000 sequencing system.

ScRNA-seq Library Generation: Droplet-based 3′ end scRNA-seq was performed by encapsulating sorted live $CD45^+$ tumor-infiltrating immune cells into droplets using the 10x Genomics platform. cDNA libraries were prepared using Chromium Single Cell 3′ Reagent Kits v3 according to the manufacturer's protocol (10x Genomics). The generated scRNA-seq libraries were sequenced using an Illumina NovaSeq 6000.

Alignment, Barcode Assignment, UMI Counting: The Cell Ranger pipeline was used to conduct sample demultiplexing, barcode processing, and single-cell 3′ counting. The Linux command *cellranger mkfastq* was applied to demultiplex raw base call (BCL) files from the illumine NovaSeq6000 sequencer, into sample-specific fastq files. Then, fastq files for each sample were processed with *cellranger count*, which was used to align samples to mm10 genome, filter and quantify.

Data Preprocessing with Seurat R Package: Seurat-guided analyses (https://satijalab.org/seurat/vignettes.html) were used to preprocess and integrate datasets from different treatment groups.[49] Genes that were expressed in less than 5 cells or cells that expressed less than 8000 and more than 6000 genes were excluded. Also, cells that expressed less than 512 and more than 92 600 counts or with a mitochondria percentage over 10% were excluded. Most variable genes were identified using the FindVariableFeatures function by setting feature numbers as 2000. Principal component analysis (PCA) was performed on the scaled matrix (with most variable genes only) using the first 30 principal components (PCs). Both tSNE and UMAP dimensional reductions were carried out using the first 20 PCs to obtain 2D representations of the cell states. For clustering, we used the function FindClusters that implements a shared nearest neighbor (SNN) modularity optimization-based clustering algorithm on 30 PCs with resolution 0.5 for default analysis.

Identification of Cluster-specific Genes and Marker-based Classification: Cells clusters were obtained by using the FindClusters function of the Seurat R package, which identifies clusters through an SNN modularity optimization–based algorithm. The biological cell type identities of each cluster were annotated with the assistance of an immune-cell scoring algorithm comparing the differentially expressed gene (DEG) signatures obtained from Seurat with the Immunological Genome Project Database (ImmGen).[50] This in silico cell type annotation was verified by using known canonical immune cell genes.

Gene Set Enrichment Analysis: Differential Gene Expression was obtained by using the FindMarkers function in Seurat. MAST was used as the methodology. Ranked gene lists were then analyzed for gene set enrichment by using the clusterProfiler R package.[47] Hallmark gene sets (H) from the Molecular Signature Database (MSigDB, https://www.gsea-msigdb.org/gsea/msigdb) were used in these analyses.[51]

Statistical Analysis: Evaluations for tumor growth and FACS data were conducted using one-way ANOVA. In conjunction with ANOVA, the post-hoc test Tukey's multiple comparisons test was used to identify significant differences between pairs of means. MAST test was used for analyzing differential gene expression in selected cell clusters. P values less than or equal to 0.05 were considered statistically significant throughout (*, $p \leq 0.05$; **, $p \leq 0.01$).

Data and Software Availability: The accession number for the scRNAseq data reported in this paper is GEO: GSE150675 (https://www.ncbi.nlm.nih.gov/geo/query/acc.cgi?acc = GSE150675).[13b] Analysis of such data can also be available upon request.

Ethics Declarations: WRC was co-founder and a member of the Board of Directors of Immunophotonics, Inc. CFW, TH, SSKL, and LA declare a conflict of interest as employees with minority ownership stakes of Immunophotonics, Inc., the manufacturer of the proprietary immunostimulant GC.

Supporting Information

Supporting Information is available from the Wiley Online Library or from the author.

Acknowledgements

A.R.H., K.L., and C.F. contributed equally to this work. This work was supported in part by the National Cancer Institute (R01CA205348 and R01CA269897), and the Oklahoma Center for the Advancement of Science and Technology (HF20-019 and HR23-069).

Conflict of Interest

The authors declare no conflict of interest.

Data Availability Statement

The data that support the findings of this study are available on request from the corresponding author. The data are not publicly available due to privacy or ethical restrictions.

Keywords

antitumor and antiviral immunities, Chitosan, interleukin 1β (IL-1β), IP-001, *N*-dihydrogalactochitosan (GC, pattern recognition receptors (PRRs), stimulator of interferon genes (STING), type I interferons (IFNs)

Received: June 10, 2024
Revised: August 22, 2024
Published online:

[1] M. B. Kaczmarek, K. Struszczyk-Swita, X. Li, M. Szczęsna-Antczak, M. Daroch, *Front. Bioeng. Biotechnol.* **2019**, *7*, 243.
[2] a) X. Li, M. Min, N. Du, Y. Gu, T. Hode, M. Naylor, D. Chen, R. E. Nordquist, W. R. Chen, *Clin. Dev. Immunol.* **2013**, *2013*, 387023; b) D. Zhao, S. Yu, B. Sun, S. Gao, S. Guo, K. Zhao, *Polymers (Basel)* **2018**, *10*, 462.
[3] E. C. Carroll, L. Jin, A. Mori, N. Muñoz-Wolf, E. Oleszycka, H. B. T. Moran, S. Mansouri, C. P. McEntee, E. Lambe, E. M. Agger, P. Andersen, C. Cunningham, P. Hertzog, K. A. Fitzgerald, A. G. Bowie, E. C. Lavelle, *Immunity* **2016**, *44*, 597.
[4] a) E. V. Vassilieva, D. W. Taylor, R. W. Compans, *Front. Immunol.* **2019**, *10*, 3006; b) E. Van Dis, K. M. Sogi, C. S. Rae, K. E. Sivick, N. H. Surh, M. L. Leong, D. B. Kanne, K. Metchette, J. J. Leong, J. R. Bruml, V. Chen, K. Heydari, N. Cadieux, T. Evans, S. M. McWhirter, T. W. Dubensky, D. A. Portnoy, S. A. Stanley, *Cell Rep.* **2018**, *23*, 1435; c) R. E. Vatner, E. M. Janssen, *Mol. Immunol.* **2019**, *110*, 13; d) Y. Zhu, X. An, X. Zhang, Y. Qiao, T. Zheng, X. Li, *Mol. Cancer* **2019**, *18*, 152.
[5] H. Wang, S. Hu, X. Chen, H. Shi, C. Chen, L. Sun, Z. J. Chen, *Proc. Natl. Acad. Sci. USA* **2017**, *114*, 1637.
[6] B. Bellich, I. D'Agostino, S. Semeraro, A. Gamini, A. Cesàro, *Mar. Drugs* **2016**, *14*, 99.
[7] W. R. Chen, R. Carubelli, H. Liu, R. E. Nordquist, *Mol. Biotechnol.* **2003**, *25*, 37.
[8] M. Korbelik, T. Hode, S. S. K. Lam, W. R. Chen, *Cells* **2021**, *10*, 492.
[9] X. Li, G. L. Ferrel, M. C. Guerra, T. Hode, J. A. Lunn, O. Adalsteinsson, R. E. Nordquist, H. Liu, W. R. Chen, *Photochem. Photobiol. Sci.* **2011**, *10*, 817.
[10] X. Li, M. F. Naylor, H. Le, R. E. Nordquist, T. K. Teague, C. A. Howard, C. Murray, W. R. Chen, *Cancer Biol. Ther.* **2010**, *10*, 1081.
[11] a) M. F. Naylor, W. R. Chen, T. K. Teague, L. A. Perry, R. E. Nordquist, *Br. J. Dermatol.* **2006**, *155*, 1287; b) W. R. Chen, S. W. Jeong, M. D. Lucroy, R. F. Wolf, E. W. Howard, H. Liu, R. E. Nordquist, *Int. J. Cancer* **2003**, *107*, 1053; c) F. Zhou, X. Li, M. F. Naylor, T. Hode, R. E. Nordquist, L. Alleruzzo, J. Raker, S. S. Lam, N. Du, L. Shi, X. Wang, W. R. Chen, *Cancer Lett.* **2015**, *359*, 169.
[12] a) F. Zhou, J. Yang, Y. Zhang, M. Liu, M. L. Lang, M. Li, W. R. Chen, *Clin. Cancer Res.* **2018**, *24*, 5335; b) A. D. Garg, S. Martin, J. Golab, P. Agostinis, *Cell Death Differ.* **2014**, *21*, 26.
[13] a) A. R. Hoover, K. Liu, C. I. DeVette, J. R. Krawic, A. D. Medcalf, C. L. West, T. Hode, S. S. K. Lam, A. L. Welm, X. H. Sun, W. H. Hildebrand, W. R. Chen, *Clin. Transl. Med.* **2022**, *12*, e937; b) K. Liu, A. R. Hoover, J. R. Krawic, C. I. DeVette, X. H. Sun, W. H. Hildebrand, M. L. Lang, R. C. Axtell, W. R. Chen, *Theranostics* **2022**, *12*, 639.
[14] D. Fong, P. Grégoire-Gélinas, A. P. Cheng, T. Mezheritsky, M. Lavertu, S. Sato, C. D. Hoemann, *Biomaterials* **2017**, *129*, 127.
[15] S. Tsuchiya, Y. Kobayashi, Y. Goto, H. Okumura, S. Nakae, T. Konno, K. Tada, *Cancer Res.* **1982**, *42*, 1530.
[16] a) L. Zitvogel, L. Galluzzi, O. Kepp, M. J. Smyth, G. Kroemer, *Nat. Rev. Immunol.* **2015**, *15*, 405; b) C. Lu, J. D. Klement, M. L. Ibrahim, W. Xiao, P. S. Redd, A. Nayak-Kapoor, G. Zhou, K. Liu, *J. Immunother. Cancer* **2019**, *7*, 157.
[17] D. B. Stetson, R. Medzhitov, *Immunity* **2006**, *25*, 373.
[18] A. R. Hoover, S. Kaabinejadian, J. R. Krawic, X. H. Sun, A. R. Naqash, Q. Yin, X. Yang, K. C. Garcia, M. M. Davis, W. H. Hildebrand, W. R. Chen, *J. Immunother. Cancer* **2022**, *10*, e004973.
[19] W. T. He, H. Wan, L. Hu, P. Chen, X. Wang, Z. Huang, Z. H. Yang, C. Q. Zhong, J. Han, *Cell Res.* **2015**, *25*, 1285.
[20] S. M. Man, R. Karki, T. D. Kanneganti, *Immunol. Rev.* **2017**, *277*, 61.
[21] M. L. G. Ramirez, M. Poreba, S. J. Snipas, K. Groborz, M. Drag, G. S. Salvesen, *J. Biol. Chem.* **2018**, *293*, 7058.
[22] a) S. Rühl, P. Broz, *Eur. J. Immunol.* **2015**, *45*, 2927; b) N. Kayagaki, I. B. Stowe, B. L. Lee, K. O'Rourke, K. Anderson, S. Warming, T. Cuellar, B. Haley, M. Roose-Girma, Q. T. Phung, P. S. Liu, J. R. Lill, H. Li, J. Wu, S. Kummerfeld, J. Zhang, W. P. Lee, S. J. Snipas, G. S. Salvesen, L. X. Morris, L. Fitzgerald, Y. Zhang, E. M. Bertram, C. C. Goodnow, V. M. Dixit, *Nature* **2015**, *526*, 666.
[23] M. Brault, T. M. Olsen, J. Martinez, D. B. Stetson, A. Oberst, *J. Immunol.* **2018**, *200*, 2748.
[24] a) X. Hu, W. Zhang, L. Wang, N. Wan, B. Wang, W. Li, H. Hua, X. Hu, F. Shan, *Hum. Vaccin. Immunother.* **2012**, *8*, 1250; b) F. Walter, E. Winter, S. Rahn, J. Heidland, S. Meier, A. M. Struzek, M. Lettau, L. M. Philipp, S. Beckinger, L. Otto, J. L. Möller, O. Helm, D. Wesch, R. Scherließ, S. Sebens, *PLoS One* **2020**, *15*, e0239369.
[25] S. R. Woo, M. B. Fuertes, L. Corrales, S. Spranger, M. J. Furdyna, M. Y. Leung, R. Duggan, Y. Wang, G. N. Barber, K. A. Fitzgerald, M. L. Alegre, T. F. Gajewski, *Immunity* **2014**, *41*, 830.
[26] J. D. Sauer, K. Sotelo-Troha, J. von Moltke, K. M. Monroe, C. S. Rae, S. W. Brubaker, M. Hyodo, Y. Hayakawa, J. J. Woodward, D. A. Portnoy, R. E. Vance, *Infect. Immun.* **2011**, *79*, 688.
[27] H. Ono, R. Ohta, Y. Kawasaki, A. Niwa, H. Takada, T. Nakahata, S. Ohga, M. K. Saito, *Inflamm. Res.* **2018**, *67*, 879.
[28] M. M. Gaidt, T. S. Ebert, D. Chauhan, K. Ramshorn, F. Pinci, S. Zuber, F. O'Duill, J. L. Schmid-Burgk, F. Hoss, R. Buhmann, G. Wittmann, E. Latz, M. Subklewe, V. Hornung, *Cell* **2017**, *171*, 1110.
[29] S. X. Ge, E. W. Son, R. Yao, *BMC Bioinformatics* **2018**, *19*, 534.
[30] M. I. Love, W. Huber, S. Anders, *Genome Biol.* **2014**, *15*, 550.
[31] M. Ashburner, C. A. Ball, J. A. Blake, D. Botstein, H. Butler, J. M. Cherry, A. P. Davis, K. Dolinski, S. S. Dwight, J. T. Eppig, M. A. Harris, D. P. Hill, L. Issel-Tarver, A. Kasarskis, S. Lewis, J. C. Matese, J. E. Richardson, M. Ringwald, G. M. Rubin, G. Sherlock, *Nat. Genet.* **2000**, *25*, 25.
[32] M. Kanehisa, S. Goto, *Nucleic Acids Res.* **2000**, *28*, 27.
[33] a) S. Yum, M. Li, Y. Fang, Z. J. Chen, *Proc. Natl. Acad. Sci. USA* **2021**, *118*, 2100225118; b) J. J. Suschak, S. Wang, K. A. Fitzgerald, S. Lu, *J. Immunol.* **2016**, *196*, 310; c) G. Dunphy, S. M. Flannery, J. F. Almine, D. J. Connolly, C. Paulus, K. L. Jønsson, M. R. Jakobsen, M. M. Nevels, A. G. Bowie, L. Unterholzner, *Mol. Cell* **2018**, *71*, 745; d) T. Abe, G. N. Barber, *J. Virol.* **2014**, *88*, 5328.
[34] J. Maelfait, L. Liverpool, A. Bridgeman, K. B. Ragan, J. W. Upton, J. Rehwinkel, *EMBO J.* **2017**, *36*, 2529.
[35] S. Kesavardhana, T. Kuriakose, C. S. Guy, P. Samir, R. K. S. Malireddi, A. Mishra, T. D. Kanneganti, *J. Exp. Med.* **2017**, *214*, 2217.
[36] H. Jiao, L. Wachsmuth, S. Kumari, R. Schwarzer, J. Lin, R. O. Eren, A. Fisher, R. Lane, G. R. Young, G. Kassiotis, W. J. Kaiser, M. Pasparakis, *Nature* **2020**, *580*, 391.
[37] L. Unterholzner, S. E. Keating, M. Baran, K. A. Horan, S. B. Jensen, S. Sharma, C. M. Sirois, T. Jin, E. Latz, T. S. Xiao, K. A. Fitzgerald, S. R. Paludan, A. G. Bowie, *Nat. Immunol.* **2010**, *11*, 997.
[38] C. Fu, A. Jiang, *Front. Immunol.* **2018**, *9*, 3059.

[39] a) P. Meiser, M. A. Knolle, A. Hirschberger, G. P. de Almeida, F. Bayerl, S. Lacher, A. M. Pedde, S. Flommersfeld, J. Hönninger, L. Stark, F. Stögbauer, M. Anton, M. Wirth, D. Wohlleber, K. Steiger, V. R. Buchholz, B. Wollenberg, C. E. Zielinski, R. Braren, D. Rueckert, P. A. Knolle, G. Kaissis, J. P. Böttcher, *Cancer Cell* **2023**, *41*, 1498; b) J. C. Cancel, K. Crozat, M. Dalod, R. Mattiuz, *Front. Immunol.* **2019**, *10*, 9.
[40] a) E. Y. Lin, A. V. Nguyen, R. G. Russell, J. W. Pollard, *J. Exp. Med.* **2001**, *193*, 727; b) S. Attalla, T. Taifour, T. Bui, W. Muller, *Oncogene* **2021**, *40*, 475; c) C. Li, X. Xu, S. Wei, P. Jiang, L. Xue, J. Wang, *J Immunother Cancer* **2021**, *9*.
[41] S. Li, M. Luo, Z. Wang, Q. Feng, J. Wilhelm, X. Wang, W. Li, J. Wang, A. Cholka, Y. X. Fu, B. D. Sumer, H. Yu, J. Gao, *Nat. Biomed. Eng.* **2021**, *5*, 455.
[42] M. Benguigui, T. J. Cooper, P. Kalkar, S. Schif-Zuck, R. Halaban, A. Bacchiocchi, I. Kamer, A. Deo, B. Manobla, R. Menachem, J. Haj-Shomaly, A. Vorontsova, Z. Raviv, C. Buxbaum, P. Christopoulos, J. Bar, M. Lotem, M. Sznol, A. Ariel, S. S. Shen-Orr, Y. Shaked, *Cancer Cell* **2024**, *42*, 253.
[43] S. Qi, L. Lu, F. Zhou, Y. Chen, M. Xu, L. Chen, X. Yu, W. R. Chen, Z. Zhang, *Theranostics* **2020**, *10*, 1814.
[44] A. M. Bolger, M. Lohse, B. Usadel, *Bioinformatics* **2014**, *30*, 2114.
[45] H. Li, B. Handsaker, A. Wysoker, T. Fennell, J. Ruan, N. Homer, G. Marth, G. Abecasis, R. Durbin, *Bioinformatics* **2009**, *25*, 2078.
[46] Y. Liao, G. K. Smyth, W. Shi, *Bioinformatics* **2014**, *30*, 923.
[47] G. Yu, L. G. Wang, Y. Han, Q. Y. He, *OMICS* **2012**, *16*, 284.
[48] B. A. Smith, D. N. Shelton, C. Kieffer, B. Milash, J. Usary, C. M. Perou, P. S. Bernard, B. E. Welm, *Genes Cancer* **2012**, *3*, 550.
[49] A. Butler, P. Hoffman, P. Smibert, E. Papalexi, R. Satija, *Nat. Biotechnol.* **2018**, *36*, 411.
[50] H. A. Ekiz, T. B. Huffaker, A. H. Grossmann, W. Z. Stephens, M. A. Williams, J. L. Round, R. M. O'Connell, *JCI Insight* **2019**, *4*.
[51] A. Liberzon, *Methods Mol. Biol.* **2014**, *1150*, 153.